



# Higgs Production at LHC

Vittorio Del Duca<sup>a</sup>

<sup>a</sup>Istituto Nazionale di Fisica Nucleare, sez. di Torino, via P. Giuria 1, 10125 - Torino, Italy

We review Higgs production at hadron colliders via vector-boson fusion and via gluon fusion, fully inclusively and in association with one and two jets. Then we address the issue of the measurement of the coupling of the Higgs to the vector bosons at LHC.

## 1 Introduction

The mechanism that governs the electroweak symmetry breaking is at present the largest unknown in the Standard Model (SM) of elementary particle physics. The canonical mechanism, the Higgs model, is a keystone of the SM and its supersymmetric extensions. However, it is based on the existence of a CP-even scalar particle, the Higgs boson, which has not been detected yet and is the most wanted particle of the Fermilab Tevatron and the CERN Large Hadron Collider (LHC) physics programmes. The direct search in the  $e^+e^- \rightarrow ZH$  process at the CERN LEP2 collider has posed a lower bound of 114.1 GeV on the SM Higgs mass,  $M_H$  [ 1, 2, 3, 4, 5]. LEP2 also posed lower bounds of 91.0 GeV (91.9 GeV) on the CP-even (CP-odd) Higgs bosons of the minimal supersymmetric extension of the Standard Model (MSSM) [ 6]. On the other hand, a SM Higgs boson with a mass of the order of 200 GeV or less is favoured by analyses of the electroweak precision data [ 7], and the upper bound on the lightest Higgs boson in the MSSM is at about 135 GeV [ 8, 9, 10]. Thus the intermediate mass region ( $M_H \lesssim 200$  GeV) seems to be preferred.

In  $pp$ -collisions, the dominant production mechanism over the entire Higgs mass range accessible at LHC is via gluon fusion  $gg \rightarrow H$ , where the coupling of the Higgs to the gluons is mediated by a heavy quark loop. If the mass of the Higgs is light ( $M_H \lesssim 150$  GeV), as one may expect from the electroweak fits to the LEP data, the most important decay mode is the rare decay into two photons,  $H \rightarrow \gamma\gamma$  [ 11, 12], characterised by a very narrow mass peak. In inclusive searches, the main Higgs decays  $H \rightarrow b\bar{b}, \tau^+\tau^-$  are overwhelmed by large QCD backgrounds.

The second largest production mechanism is via weak-boson fusion (WBF)  $qq \rightarrow qqH$ . In terms of significance, *i.e.* ratio of signal over root of background  $S/\sqrt{B}$ , Higgs production via WBF is large as (or larger than) the one via gluon fusion [ 13]. In addition, it allows for the study of the Higgs couplings to gauge bosons and fermions [ 14] at LHC, because of the coupling to the weak bosons in the production mode and because of the different decay modes which can be observed experimentally [ 13],  $H \rightarrow \gamma\gamma$  [ 15],  $H \rightarrow WW$  [ 16, 17] and  $H \rightarrow \tau\tau$  [ 18, 19].

Firstly, we review in general Higgs production via WBF and via gluon fusion, and then we consider both in association with two jets, as regards the Higgs-vector-boson couplings.

## 2 Higgs Production via Vector Boson Fusion

Higgs production via WBF  $qq \rightarrow qqH$  occurs as the scattering between two (anti)quarks with weak-boson ( $W$  or  $Z$ ) exchange in the  $t$ -channel and with the Higgs boson radiated off the weak-boson propagator, Fig. 1. Since the distribution functions of the incoming valence quarks peak at values of the momentum fractions  $x \approx 0.1$  to  $0.2$ , Higgs production via WBF tends to produce naturally two highly energetic outgoing quarks. In addition, since the weak-boson mass provides a natural cutoff on the weak-boson propagator, two jets with a transverse energy typically of the order of a fraction of the weak-boson mass can be easily produced. Thus a large fraction of the events of the total cross section for Higgs production via WBF occurs with two jets with a large rapidity interval between them, typically one at forward and the other at backward rapidities. As we shall see, this feature can be used in order to distinguish Higgs production via WBF from the one via gluon fusion.

Another feature of WBF is that, except for the Higgs decay products, which may be hadronic, no hadron production occurs in the rapidity interval between the jets, because the weak boson exchanged in the  $t$ -channel is colourless [ 20, 21]: to  $O(\alpha_s)$ , gluon radiation occurs only as bremsstrahlung off the quark legs (since no colour is exchanged in the  $t$ -channel in the Born process, no gluon exchange is possible to  $O(\alpha_s)$ , except for a tiny contribution due to equal-flavour quark scattering with  $t \leftrightarrow u$  channel exchange). Next-to-leading order (NLO) corrections in  $\alpha_s$  to Higgs production via WBF have been computed for the total cross section [ 22] and for Higgs production in association with two jets [ 23]. They have been found to be typically modest, of the order of 5 to 10%. Thus Higgs production via WBF is under a good theoretical control.

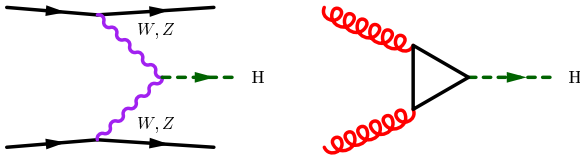


Figure 1. Higgs production via WBF and via gluon fusion.

### 3 Higgs Production via Gluon Fusion

In the gluon fusion channel  $gg \rightarrow H$ , the Higgs couples to the gluons through a heavy quark loop, Fig. 1. In the SM, the leading contribution comes from the top quark, the contributions from other quarks being at least smaller by a factor  $O(M_b^2/M_{\text{top}}^2)$ . Since the Higgs boson is produced via a loop, a calculation of the production rate is quite involved, even at leading order in  $\alpha_s$ . The production rate for  $gg \rightarrow H$  has been computed to NLO in  $\alpha_s$ , including the heavy quark mass dependence [24, 25] (which required an evaluation at two-loop accuracy). The NLO QCD corrections are large and increase the production rate by up to 80%. However, the coupling of the Higgs to the gluons via a top-quark loop can be replaced by an effective coupling [26, 27], called the *large  $M_{\text{top}}$  limit*, if the Higgs mass is smaller than the threshold for the creation of a top-quark pair,  $M_H \lesssim 2M_{\text{top}}$ . That simplifies calculations tremendously, because it effectively reduces the number of loops in a given diagram by one. It has been shown that adding the NLO QCD corrections in the large  $M_{\text{top}}$  limit to the leading order calculation with the top quark mass dependence approximates the full NLO QCD corrections within 10% up to 1 TeV [28] covering the entire Higgs mass range at the LHC. The reason for the good quality of this approximation is that the QCD corrections to  $gg \rightarrow H$  are dominated by soft gluon effects, which do not resolve the top-quark loop mediating the coupling of the Higgs boson to the gluons. The next-to-next-to-leading order (NNLO) corrections to the production rate for  $gg \rightarrow H$  have been evaluated in the large  $m_t$  limit [29, 30, 31] and display an increase of about 15% at  $M_H = 120$  GeV with respect to the NLO evaluation, Fig. 2. The dominant part of the NNLO corrections comes from the gluon and collinear radiation [32, 33], in agreement with what already observed at NLO. In addition, the threshold resummation of soft gluon effects [28, 34] enhances the NNLO result by about 5%, showing that the calculation stabilises at NNLO.

For a light Higgs ( $M_H \lesssim 150$  GeV), the most relevant decay mode is into two photons,  $H \rightarrow \gamma\gamma$ . The irreducible  $pp \rightarrow \gamma\gamma$  background proceeds at leading order via the sub-process  $q\bar{q} \rightarrow \gamma\gamma$ , which is independent of  $\alpha_s$ . The NLO corrections to  $pp \rightarrow \gamma\gamma$  are known [35, 36, 37]. They are incorporated in the program DIPHOX, which includes all relevant photon fragmentation effects [38]. The NLO corrections are very large, because the formally

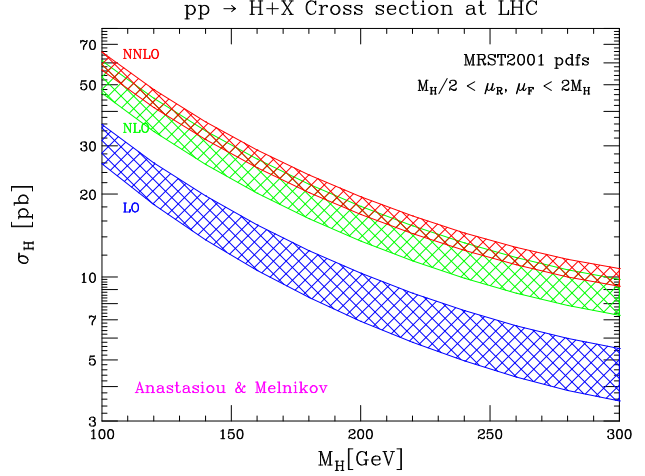


Figure 2. Higgs production via gluon fusion in  $pp$  collisions at  $\sqrt{S} = 14$  TeV as a function of the Higgs mass, from Ref. [30]. The production rate has been computed in the large  $M_{\text{top}}$  limit, to leading order, NLO and NNLO accuracy. The shaded bands display the renormalisation  $\mu_R$  and factorisation  $\mu_F$  scale variations. The lower contours correspond to  $\mu_R = 2M_H$  and  $\mu_F = M_H/2$ ; the upper contours to  $\mu_R = M_H/2$  and  $\mu_F = 2M_H$ .

higher order sub-processes involving gluons in the initial state can be as large as the leading order contribution, since the gluon distribution in the proton decreases monotonically with its momentum fraction  $x$ . Thus the  $qg \rightarrow \gamma\gamma q$ , occurring first to NLO, dominates the NLO corrections. In fact, the quark-loop mediated sub-process  $gg \rightarrow \gamma\gamma$  [39, 40], which is  $O(\alpha_s^2)$  and thus formally belongs to the NNLO corrections, contributes about 50% to the  $\gamma\gamma$  background [41]. However, since  $gg \rightarrow \gamma\gamma$  occurs first at  $O(\alpha_s^2)$ , it is effectively a leading order calculation to that order, and thus it bears a large dependence on renormalisation and factorisation scales. In order to reduce that uncertainty, the NLO corrections to  $gg \rightarrow \gamma\gamma$  (which are  $O(\alpha_s^3)$  and thus formally belong to the NNNLO corrections) have been evaluated [42]. They were found to be modest, increasing the overall irreducible  $pp \rightarrow \gamma\gamma$  background by less 10% over the relevant diphoton mass spectrum,  $m_{\gamma\gamma} \gtrsim 100$  GeV. Other NNLO corrections to the irreducible  $pp \rightarrow \gamma\gamma$  background, like the sub-process  $gg \rightarrow \gamma\gamma q\bar{q}$  and the  $O(\alpha_s)$  corrections to  $qg \rightarrow \gamma\gamma q$ , might be numerically relevant, so a full NNLO evaluation of the irreducible  $pp \rightarrow \gamma\gamma$  background is desirable.

#### 3.1 Higgs + 1 Jet Production

For a light Higgs, a process that promises to have a more amenable background is Higgs production in association with a high transverse energy ( $E_T$ ) jet,  $pp \rightarrow H + \text{jet} \rightarrow \gamma\gamma + \text{jet}$ . In addition, this process offers the advantage of being more flexible with respect to choosing suitable acceptance cuts to curb the background. The  $pp \rightarrow H + \text{jet}$  process is known to leading order exactly [43]. The

contributing subprocesses include quark-gluon scattering which is mediated by top-quark triangles, and gluon-gluon scattering which requires box diagrams. As regards the NLO contribution, only the bremsstrahlung corrections are known [44, 45]. However, the full NLO corrections [46, 47, 48, 49] have been evaluated in the large  $M_{\text{top}}$  limit. For Higgs + one jet production, the large  $M_{\text{top}}$  limit is valid as long as  $M_H \lesssim 2M_{\text{top}}$  and the transverse energy is smaller than the top-quark mass,  $E_T \lesssim M_{\text{top}}$  [50], and is insensitive to the jet-Higgs invariant mass becoming larger than  $M_{\text{top}}$  [51]. At  $M_H = 120$  GeV, the NLO corrections to the  $pp \rightarrow H + \text{jet}$  process increase the leading order prediction by about 60%, and thus are of the same order as the NLO corrections to fully inclusive  $pp \rightarrow H$  production considered above. At present, the NNLO corrections to  $pp \rightarrow H + \text{jet}$  are not known.

The irreducible  $pp \rightarrow \gamma\gamma \text{ jet}$  background has been analysed at leading order in Ref. [52]. It proceeds via the subprocesses  $q\bar{q} \rightarrow \gamma\gamma g$  and  $qg \rightarrow \gamma\gamma q$ , which are  $O(\alpha_s)$ , and is dominated by  $qg \rightarrow \gamma\gamma q$ , which benefits from the large gluon luminosity. The quark-loop mediated  $gg \rightarrow g\gamma\gamma$  subprocess, which is  $O(\alpha_s^3)$  and thus formally belongs to the NNLO corrections, yields a contribution to  $pp \rightarrow \gamma\gamma \text{ jet}$  which increases the leading order prediction by less than 20% [41, 53], thus it is under good theoretical control. The full NLO QCD corrections to the irreducible  $pp \rightarrow \gamma\gamma \text{ jet}$  background have been computed [54] using a “smooth” photon isolation prescription [55] which does not require a photon fragmentation contribution. They have been found to depend strongly on the photon isolation parameters. In particular, choosing a small photon isolation cone radius  $R_\gamma = 0.4$  (which is nowadays the experimental preferred choice) results in more than 100 % corrections.

## 4 Higgs + 2 Jet Production

A key component of the program to measure Higgs boson couplings at the LHC is the WBF process,  $qq \rightarrow qqH$  via  $t$ -channel  $W$  or  $Z$  exchange, characterized by two forward quark jets [14]. The NLO corrections to Higgs production via WBF fusion in association with two jets are known to be small [23] and, hence, this process promises small systematic errors.  $H + 2 \text{ jet}$  production via gluon fusion, while part of the inclusive Higgs signal, constitutes a background when trying to isolate the  $HWW$  and  $HZZ$  couplings responsible for the WBF process. A precise description of this background is needed in order to separate the two major sources of  $H + 2 \text{ jet}$  events: one needs to find characteristic distributions which distinguish the WBF process from gluon fusion.

$H + 2 \text{ jet}$  production via gluon fusion is known at leading order exactly [44, 45]. The contributing subprocesses include quark-quark scattering which involves top-quark triangles, quark-gluon scattering which is mediated by triangles and boxes, and gluon-gluon scattering which requires

up to pentagon diagrams, Fig. 3. The relevant (squared) energy scales in the process  $pp \rightarrow j_1 j_2 H$  are the parton centre-of-mass energy  $s$ , the Higgs mass  $M_H^2$ , the dijet invariant mass  $s_{j_1 j_2}$ , and the jet-Higgs invariant masses  $s_{j_1 H}$  and  $s_{j_2 H}$ . At leading order they are related through momentum conservation,

$$s = s_{j_1 j_2} + s_{j_1 H} + s_{j_2 H} - M_H^2. \quad (1)$$

The NLO corrections to  $H + 2 \text{ jet}$  production via gluon fusion are not known.

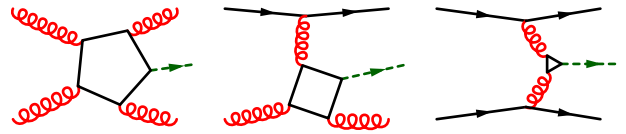


**Figure 3.**  $H + 2 \text{ jet}$  production via gluon fusion. Examples of Feynman diagrams which contribute to gluon-gluon, quark-gluon and quark-quark scattering, respectively.

In fact, in Higgs +  $n$  jet production, up to  $(n + 3)$ ,  $(n + 2)$  and  $(n + 1)$ -side polygon quark loops occur in gluon-gluon, quark-gluon and quark-quark scattering, respectively. Clearly, the complexity of the calculation discourages one from carrying on this path. For instance, the evaluation of the NLO corrections to Higgs + two jet production would imply the calculation of up to hexagon quark loops and two-loop pentagon quark loops, which are at present unfeasible. Fortunately, the calculations become simpler in two instances:

- the large  $M_{\text{top}}$  limit, in which, as we described in Sect. 3, the heavy quark loop is replaced by an effective coupling, thus reducing the number of loops in a given diagram by one;
- the high-energy limits, in which the number of sides in the largest polygon quark loop is diminished at least by one.

In order to use the large  $M_{\text{top}}$  limit, in addition to the necessary condition  $M_H \lesssim 2M_{\text{top}}$ , the Higgs and jets transverse energies must be smaller than the top-quark mass, just as it was in the context of Higgs + one jet production, Sect. 3.1. Then the kinematics allow us to consider two possible high energy limits: (a)  $s_{j_1 j_2} \gg s_{j_1 H}, s_{j_2 H} \gg M_H^2$ , i.e. the Higgs boson is centrally located in rapidity between the two jets, and very far from either jet; (b)  $s_{j_1 j_2}, s_{j_2 H} \gg s_{j_1 H}, M_H^2$ , i.e. the Higgs boson is close to jet  $j_1$  in rapidity, and both of these are very far from jet  $j_2$ . In both cases the scattering amplitudes factorize into effective vertices connected by a gluon exchanged in the  $t$  channel. Using the exact results [44, 45] as a benchmark, the large  $M_{\text{top}}$  limit and the high-energy limits above have been explored [51]. It

has been found that the high-energy factorization is independent of the large  $M_{\text{top}}$  limit: the high-energy and large  $M_{\text{top}}$  limits commute at the level of the scattering amplitude. In the high-energy limit, the sensitivity to the full  $M_{\text{top}}$  dependence occur only locally in rapidity at the level of the high-energy coefficient function for Higgs production. The issue of the conditions under which it is possible to use the high-energy and large  $M_{\text{top}}$  limits becomes important in the context of its companion process: the isolation of Higgs production via WBF requires selecting on events with large dijet invariant mass (this cut suppresses the gluon-gluon fusion contribution and reduces the QCD backgrounds). The analysis above warrants the use of the large  $M_{\text{top}}$  limit in gluon-gluon fusion, without regard to the value of the Higgs-jet and/or dijet invariant masses.

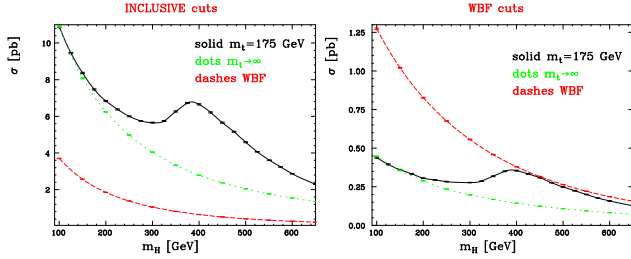


**Figure 4.**  $H + 2$  jet cross sections in  $pp$  collisions at  $\sqrt{s} = 14$  TeV as a function of the Higgs mass, from Ref. [44]. The solid and dotted lines correspond to the gluon-fusion processes induced by a top-quark loop with  $M_{\text{top}} = 175$  GeV and in the large  $M_{\text{top}}$  limit, respectively. The dashed line corresponds to weak-boson fusion. The two panels correspond to two sets of jet cuts: inclusive selection, Eq. (2), and WBF selection, Eqs. (2) and (3).

In the left-hand side panel of Fig. 4, we consider  $H + 2$  jet production at LHC as a function of the Higgs mass. In the exact curve for gluon fusion,  $M_{\text{top}} = 175$  GeV has been used (we shall use that as the default value in the plots which follow). On the jets, the following cuts are applied,

$$p_{Tj} > 20 \text{ GeV}, \quad |\eta_j| < 5, \quad R_{jj} > 0.6, \quad (2)$$

where  $p_{Tj}$  is the transverse momentum of a final state jet and  $R_{jj}$  describes the separation of the two partons in the pseudo-rapidity  $\eta$  versus azimuthal angle plane. A conspicuous feature (familiar from the inclusive gluon-fusion cross section) of the exact  $H + 2$  jet gluon-fusion cross section in Fig. 4 is the threshold enhancement at  $m_H \approx 2m_t$ . The gluon-fusion contribution dominates over the whole Higgs mass spectrum because the cuts (2) retain events with jets in the central region, with relatively small dijet invariant mass. As explained in Sect. 2, a large fraction of Higgs production via WBF occurs with two jets with a large rapidity interval between them. Thus in order to isolate Higgs production via WBF from the same via gluon-gluon fusion, we must select events with a large dijet invariant mass [

16, 19]. Thus, in addition to the cuts of Eq. (2), on the right-hand side panel of Fig. 4 we require

$$|\eta_{j1} - \eta_{j2}| > 4.2, \quad \eta_{j1} \cdot \eta_{j2} < 0, \quad m_{jj} > 600 \text{ GeV}, \quad (3)$$

i.e. the two tagging jets must be well separated in rapidity, they must reside in opposite detector hemispheres and they must possess a large dijet invariant mass. With these selection cuts the WBF processes dominate over gluon fusion by about 3/1 for Higgs masses in the 100 to 200 GeV range. A further suppression of gluon fusion as compared to WBF cross sections is to be expected with a central-jet veto [18, 56, 57], which can be used to suppress semi-soft gluon radiation. This means that a relatively clean separation of WBF and gluon-fusion processes will be possible at LHC.

As a caveat, we must note that the  $H + 2$  jet gluon-fusion cross section displays a strong dependence on the renormalisation scale  $\mu_R$ : that is because it is a leading-order calculation to  $\mathcal{O}(\alpha_s^4)$ . The only way to ameliorate this problem is to compute the NLO corrections. As we discussed above, with the present-day technology an exact NLO calculation is not feasible. However, the NLO corrections could be computed in the large  $M_{\text{top}}$  limit.

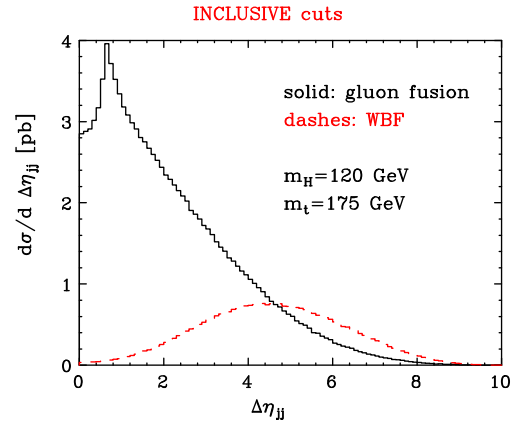


**Figure 5.** Distribution in the rapidity difference  $\Delta\eta_{jj}$  between the two jets, from Ref. [45]. The solid and dashed lines correspond to the gluon-fusion and WBF processes, respectively. The cuts of Eq. (2) have been used.

To substantiate our claim that Higgs production via WBF tends to yield spontaneously two jets with a large rapidity interval between them, in Fig. 5 we show the distribution in the rapidity difference  $\Delta\eta_{jj}$  between the two jets, using the cuts of Eq. (2), for  $M_H = 120$  GeV. While the gluon-fusion cross section decreases monotonically (the peak at small  $\Delta\eta_{jj}$  is an artifact of the cut on  $R_{jj}$ ), the WBF cross section produces naturally two jets at rather large  $\Delta\eta_{jj}$ .

Another discriminant between gluon fusion and WBF is the correlation between the two jets on the azimuthal plane.



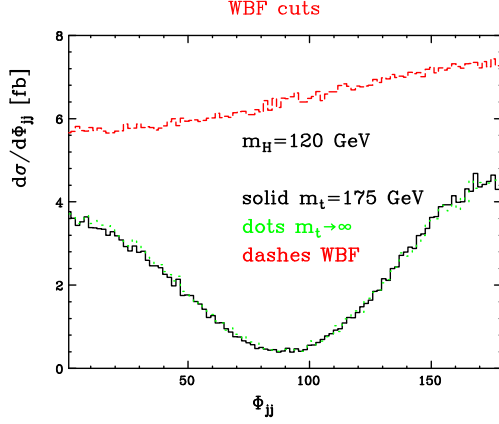


**Figure 6.** Distribution in the azimuthal angle  $\Delta\phi_{jj}$  between the two jets, from Ref. [ 45]. The solid and dotted lines correspond to the gluon-fusion processes with  $M_{\text{top}} = 175$  GeV and in the large  $M_{\text{top}}$  limit, respectively. The dashed line corresponds to weak-boson fusion. The cuts of Eqs. (2) and (3) have been used.

It can be shown [ 45] that while the scattering amplitudes for WBF have a rather mild dependence on the azimuthal angle  $\Delta\phi_{jj}$  between the jets, the ones for gluon fusion have an approximate zero at  $\Delta\phi_{jj} = \pi/2$ . In Fig. 6 we show the distribution in  $\Delta\phi_{jj}$ <sup>1</sup>. Note that, even with the cuts of Eq. (3), the large  $M_{\text{top}}$  limit approximates very well the exact curve, in accordance with the discussion on the high-energy and the large- $M_{\text{top}}$  limits above.

The distribution in the azimuthal angle  $\Delta\phi_{jj}$  between the two jets can be used as a tool to investigate the tensor structure of the coupling between the Higgs and the vector bosons [ 60]. For example, let us suppose that there is an anomalous  $WWH$  coupling. This could be modelled by a gauge-invariant effective Lagrangian, which, after expanding the Higgs field about the v.e.v., would be given in terms of dimension 5 operators as follows,

$$\mathcal{L}_5 = \frac{1}{\Lambda_{e,5}} H W_{\mu\nu}^+ W^{-\mu\nu} + \frac{1}{\Lambda_{o,5}} H \tilde{W}_{\mu\nu}^+ W^{-\mu\nu} \quad (4)$$

with  $W^{\mu\nu}$  ( $\tilde{W}^{\mu\nu}$ ) the vector-boson field-strength (axial) tensor and  $\Lambda_{e,5}$  ( $\Lambda_{o,5}$ ) the CP-even (odd) coupling<sup>2</sup>. In Fig. 7, the distribution in  $\Delta\phi_{jj}$  is shown for the SM and the anomalous couplings, assuming that a Higgs-like scalar signal is found at LHC at the same rate as the SM one. In this respect,  $H + 2$  jet from gluon fusion would yield an undesired interference, because the effective Lagrangian which

<sup>1</sup>A subsequent analysis of the distribution in  $\Delta\phi_{jj}$ , based on generating the two jets and additional gluon radiation through the event generator HERWIG [ 58], has found a much milder correlation in  $H + 2$  jet from gluon fusion [ 59]. Unfortunately, since in that case also the two jets were generated through the parton shower, we have no way of comparing directly the analysis of Ref. [ 59] to Fig. 6.

<sup>2</sup>The Lagrangian of Eq. (4) breaks the  $SU(2) \otimes U(1)$  invariance, but here we are not concerned with the consistency of the underlying fundamental theory. Rather, we want to provide a tool to distinguish between different possible couplings, wherever they might be come from.

models gluon fusion in the large  $M_{\text{top}}$  limit is a CP-even dimension 5 operator of the same form as the one in Eq. (4). Thus, there is a significant systematic uncertainty due to the poor determination of the normalisation of  $H + 2$  jet from gluon fusion, which is only known at leading order. The state of the affairs would be greatly improved with a calculation of the corresponding NLO corrections.

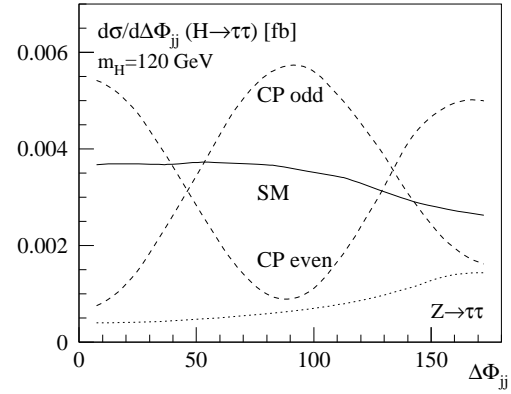


**Figure 7.** Distribution in  $\Delta\phi_{jj}$  for  $H + 2$  jet production via WBF, with the Higgs decaying into a  $\tau\tau$  pair, from Ref. [ 60]. The solid line corresponds to the Standard Model  $WWH$  coupling, the dashed lines correspond to CP-even and CP-odd anomalous couplings. The major background  $Z + 2$  jets, with  $Z$  decaying into  $\tau\tau$ , is also represented. The cuts of Eqs. (2) and (3) have been used.

## Acknowledgments

It is a pleasure to thank W.B. Kilgore, F. Maltoni, Z. Nagy, C. Oleari, C. R. Schmidt, Z. Trocsanyi and D. Zeppenfeld for many fruitful collaborations.

## References

1. R. Barate *et al.* [ALEPH Collaboration], Phys. Lett. B **495** (2000) 1 [arXiv:hep-ex/0011045].
2. M. Acciarri *et al.* [L3 Collaboration], Phys. Lett. B **508** (2001) 225 [arXiv:hep-ex/0012019].
3. G. Abbiendi *et al.* [OPAL Collaboration], Phys. Lett. B **499** (2001) 38 [arXiv:hep-ex/0101014].
4. P. Abreu *et al.* [DELPHI Collaboration], Phys. Lett. B **499** (2001) 23 [arXiv:hep-ex/0102036].
5. [LEP Higgs Working Group for Higgs boson searches Collaboration], arXiv:hep-ex/0107029.
6. [LEP Higgs Working Group Collaboration], arXiv:hep-ex/0107030.
7. P. Gambino, arXiv:hep-ph/0311257.
8. M. Carena, H. E. Haber, S. Heinemeyer, W. Hollik, C. E. Wagner and G. Weiglein, Nucl. Phys. B **580** (2000) 29 [arXiv:hep-ph/0001002].

9. J. R. Espinosa and R. J. Zhang, Nucl. Phys. B **586** (2000) 3 [arXiv:hep-ph/0003246].
10. A. Brignole, G. Degrossi, P. Slavich and F. Zwirner, Nucl. Phys. B **631** (2002) 195 [arXiv:hep-ph/0112177].
11. CMS Collaboration, Technical Proposal, Report No. CERN/LHCC 94-38 (1994)
12. ATLAS Collaboration, Detector and Physics Performance Technical Design Report, Vol. II, Report No. CERN/LHCC 99-15 (1999).
13. S. Asai *et al.*, ATLAS Collaboration, Report No. SN-ATLAS-2003-024.
14. D. Zeppenfeld, R. Kinnunen, A. Nikitenko and E. Richter-Was, Phys. Rev. D **62** (2000) 013009 [arXiv:hep-ph/0002036].
15. D. Rainwater and D. Zeppenfeld, JHEP **9712**, 005 (1997) [arXiv:hep-ph/9712271].
16. D. Rainwater and D. Zeppenfeld, Phys. Rev. D **60**, 113004 (1999) [Erratum-ibid. D **61**, 099901 (2000)] [arXiv:hep-ph/9906218].
17. N. Kauer, T. Plehn, D. Rainwater and D. Zeppenfeld, Phys. Lett. B **503** (2001) 113 [arXiv:hep-ph/0012351].
18. D. Rainwater, D. Zeppenfeld and K. Hagiwara, Phys. Rev. D **59**, 014037 (1999) [arXiv:hep-ph/9808468].
19. T. Plehn, D. Rainwater and D. Zeppenfeld, Phys. Rev. D **61** (2000) 093005 [arXiv:hep-ph/9911385].
20. Y. L. Dokshitzer, S. I. Troian and V. A. Khoze, Sov. J. Nucl. Phys. **46** (1987) 712.
21. J. D. Bjorken, Phys. Rev. **D47** (1993) 101.
22. T. Han and S. Willenbrock, Phys. Lett. **B273**, 167 (1991).
23. T. Figy, C. Oleari and D. Zeppenfeld, Phys. Rev. D **68** (2003) 073005 [arXiv:hep-ph/0306109].
24. D. Graudenz, M. Spira and P. M. Zerwas, Phys. Rev. Lett. **70** (1993) 1372.
25. M. Spira, A. Djouadi, D. Graudenz and P. M. Zerwas, Nucl. Phys. B **453** (1995) 17 [arXiv:hep-ph/9504378].
26. M. A. Shifman, A. I. Vainshtein, M. B. Voloshin and V. I. Zakharov, Sov. J. Nucl. Phys. **30** (1979) 711.
27. J. Ellis, M. K. Gaillard and D. V. Nanopoulos, Nucl. Phys. **B106** (1976) 292.
28. M. Kramer, E. Laenen and M. Spira, Nucl. Phys. B **511** (1998) 523 [arXiv:hep-ph/9611272].
29. R. V. Harlander and W. B. Kilgore, Phys. Rev. Lett. **88** (2002) 201801 [arXiv:hep-ph/0201206].
30. C. Anastasiou and K. Melnikov, Nucl. Phys. B **646** (2002) 220 [arXiv:hep-ph/0207004].
31. V. Ravindran, J. Smith and W. L. van Neerven, Nucl. Phys. B **665** (2003) 325 [arXiv:hep-ph/0302135].
32. S. Catani, D. de Florian and M. Grazzini, JHEP **0105** (2001) 025 [arXiv:hep-ph/0102227].
33. R. V. Harlander and W. B. Kilgore, Phys. Rev. D **64** (2001) 013015 [arXiv:hep-ph/0102241].
34. S. Catani, D. de Florian, M. Grazzini and P. Nason, JHEP **0307** (2003) 028 [arXiv:hep-ph/0306211].
35. P. Aurenche, A. Douiri, R. Baier, M. Fontannaz and D. Schiff, Z. Phys. C **29** (1985) 459.
36. B. Bailey, J. F. Owens and J. Ohnemus, Phys. Rev. D **46** (1992) 2018.
37. B. Bailey and J. F. Owens, Phys. Rev. D **47** (1993) 2735.
38. T. Binoth, J. P. Guillet, E. Pilon and M. Werlen, Eur. Phys. J. C **16** (2000) 311 [arXiv:hep-ph/9911340].
39. L. Ametller, E. Gava, N. Paver and D. Treleani, Phys. Rev. D **32** (1985) 1699.
40. D. A. Dicus and S. S. Willenbrock, Phys. Rev. D **37** (1988) 1801.
41. D. de Florian and Z. Kunszt, Phys. Lett. B **460** (1999) 184 [arXiv:hep-ph/9905283].
42. Z. Bern, L. Dixon and C. Schmidt, Phys. Rev. D **66** (2002) 074018 [arXiv:hep-ph/0206194].
43. R. K. Ellis, I. Hinchliffe, M. Soldate and J. J. van der Bij, Nucl. Phys. **B297** (1988) 221.
44. V. Del Duca, W. Kilgore, C. Oleari, C. Schmidt and D. Zeppenfeld, Phys. Rev. Lett. **87** (2001) 122001 [arXiv:hep-ph/0105129].
45. V. Del Duca, W. Kilgore, C. Oleari, C. Schmidt and D. Zeppenfeld, Nucl. Phys. B **616** (2001) 367 [arXiv:hep-ph/0108030].
46. D. de Florian, M. Grazzini and Z. Kunszt, Phys. Rev. Lett. **82** (1999) 5209 [arXiv:hep-ph/9902483].
47. V. Ravindran, J. Smith and W. L. Van Neerven, Nucl. Phys. B **634** (2002) 247 [arXiv:hep-ph/0201114].
48. C. J. Glosser and C. R. Schmidt, JHEP **0212** (2002) 016 [arXiv:hep-ph/0209248].
49. J. M. Campbell and R. K. Ellis, <http://mcfm.fnal.gov/mcfm.ps>.
50. U. Baur and E. W. N. Glover, Nucl. Phys. B **339**, 38 (1990).
51. V. Del Duca, W. Kilgore, C. Oleari, C. R. Schmidt and D. Zeppenfeld, Phys. Rev. D **67** (2003) 073003 [arXiv:hep-ph/0301013].
52. S. Abdullin, M. Dubinin, V. Ilyin, D. Kovalenko, V. Savrin and N. Stepanov, Phys. Lett. B **431** (1998) 410 [arXiv:hep-ph/9805341].
53. C. Balazs, P. Nadolsky, C. Schmidt and C. P. Yuan, Phys. Lett. B **489** (2000) 157 [arXiv:hep-ph/9905551].
54. V. Del Duca, F. Maltoni, Z. Nagy and Z. Trocsanyi, JHEP **0304** (2003) 059 [arXiv:hep-ph/0303012].
55. S. Frixione, Phys. Lett. B **429** (1998) 369 [arXiv:hep-ph/9801442].
56. A. Duff and D. Zeppenfeld, Phys. Rev. D **50** (1994) 3204 [arXiv:hep-ph/9312357].
57. V. D. Barger, R. J. N. Phillips and D. Zeppenfeld, Phys. Lett. B **346** (1995) 106 [arXiv:hep-ph/9412276].
58. G. Marchesini and B. R. Webber, Nucl. Phys. B **238** (1984) 1.
59. K. Odagiri, JHEP **0303** (2003) 009 [arXiv:hep-ph/0212215].
60. T. Plehn, D. Rainwater and D. Zeppenfeld, Phys. Rev. Lett. **88** (2002) 051801 [arXiv:hep-ph/0105325].